Ore Geology Reviews 119 (2020) 103392

Contents lists available at ScienceDirect

Ore Geology Reviews

journal homepage: www.elsevier.com/locate/oregeorev

Chemostratigraphy of deep-sea sediments in the western North Pacific Ocean: Implications for genesis of mud highly enriched in rare-earth elements and yttrium

Erika Tanaka[a], Kentaro Nakamura[a,*], Kazutaka Yasukawa[b,a,c], Kazuhide Mimura[a], Koichiro Fujinaga[c,b], Koichi Iijima[d], Tatsuo Nozaki[d,b,e,c], Yasuhiro Kato[b,a,c,d,*]

[a] Department of Systems Innovation, School of Engineering, The University of Tokyo, 7-3-1 Hongo, Bunkyo-ku, Tokyo 113-8656, Japan
[b] Frontier Research Center for Energy and Resources, School of Engineering, The University of Tokyo, 7-3-1 Hongo, Bunkyo-ku, Tokyo 113-8656, Japan
[c] Ocean Resources Research Center for Next Generation, Chiba Institute of Technology, 2-17-1 Tsudanuma, Narashino, Chiba 275-0016, Japan
[d] Submarine Resources Research Center, Research Institute for Marine Resources Utilization, Japan Agency for Marine-Earth Science and Technology (JAMSTEC), 2-15 Natsushima-cho, Yokosuka, Kanagawa 237-0061, Japan
[e] Department of Planetology, Graduate School of Science, Kobe University, 1-1 Rokkodai-cho, Nada-ku, Kobe, Hyogo 657-8501, Japan

ARTICLE INFO

Keywords:
REY-rich mud
Chemostratigraphy
Minamitorishima Island
Bottom current
Pelagic clay

ABSTRACT

Deep-sea sediments containing high concentrations of rare-earth elements and yttrium (REY), termed REY-rich mud, are widely distributed in the Pacific and Indian oceans. Mud layers with very high total REY (ΣREY) concentrations (> 5000 ppm of ΣREY with ~1000 ppm of heavy rare-earth elements) have been discovered within the Japanese exclusive economic zone surrounding Minamitorishima Island, western North Pacific. The number of highly REY-enriched layers in the sediment column, the depths at which the layers occur, and the maximum ΣREY values of the layers are, however, quite variable on a scale of several tens of kilometers. The factors controlling the formation and distribution of the REY-enriched layers are still poorly understood. Here, we produce a chemostratigraphic scheme for 1240 sediment samples from 49 piston cores collected within the Minamitorishima exclusive economic zone. Detailed investigation of the bulk sediment geochemistry, which exhibits distinctive compositional data structures in multi-elemental subspaces, revealed that the samples can be categorized into five units (Units I to V) in addition to REY peaks (> 2000 ppm). These units appear in a consistent stratigraphic sequence in the studied cores. This chemostratigraphy reveals that highly REY-enriched layers formed at least three times, and that almost all of these layers were accompanied by erosion during deposition. Our results suggest that erosion events of deep-sea sediment play an important role in the formation of highly REY-rich mud layers.

1. Introduction

It has been recognized that deep-sea sediments containing high concentrations of rare earth elements and yttrium (REY), termed "REY-rich mud", are widely distributed in the Pacific Ocean (Kato et al., 2011; Yasukawa et al., 2016). REY-rich mud has also been reported from the Indian and Atlantic oceans (Menendez et al., 2017; Yasukawa et al., 2014). Kato et al. (2011) defined REY-rich mud as sediment with a total REY (ΣREY) concentration of more than 400 ppm and pointed out that this type of mud has high REY resource potential, especially for heavy rare-earth elements (HREE). More recently, Iijima et al. (2016) reported the presence of REY-rich mud containing 6800 ppm of ΣREY, including > 1100 ppm of HREE, within the Japanese exclusive economic zone (EEZ) around Minamitorishima Island in the western North Pacific Ocean (Fig. 1). Iijima et al. (2016) further classified the REY-rich mud into "ordinary REY-rich mud" (ΣREY = 400–2000 ppm), "highly REY-rich mud" (ΣREY = 2000–5000 ppm) and "extremely REY-rich mud" (ΣREY > 5000 ppm). This exceptional REY enrichment can be attributed to anomalous accumulations of biogenic calcium phosphate (BCP; Fujinaga et al., 2016; Iijima et al., 2016; Ohta et al., 2016), mainly as bones or teeth of marine vertebrates, which contain very high REY concentrations (Arrhenius et al., 1957; Bernat, 1975; Kashiwabara et al., 2014, 2018; Toyoda et al., 1990). A recent study using laser-ablation inductively coupled plasma mass spectrometry demonstrated

* Corresponding authors at: Frontier Research Center for Energy and Resources, School of Engineering, The University of Tokyo, 7-3-1 Hongo, Bunkyo-ku, Tokyo 113-8656, Japan (Y. Kato).
E-mail addresses: kentaron@sys.t.u-tokyo.ac.jp (K. Nakamura), ykato@sys.t.u-tokyo.ac.jp (Y. Kato).

https://doi.org/10.1016/j.oregeorev.2020.103392
Received 30 January 2019; Received in revised form 31 January 2020; Accepted 5 February 2020
Available online 06 February 2020

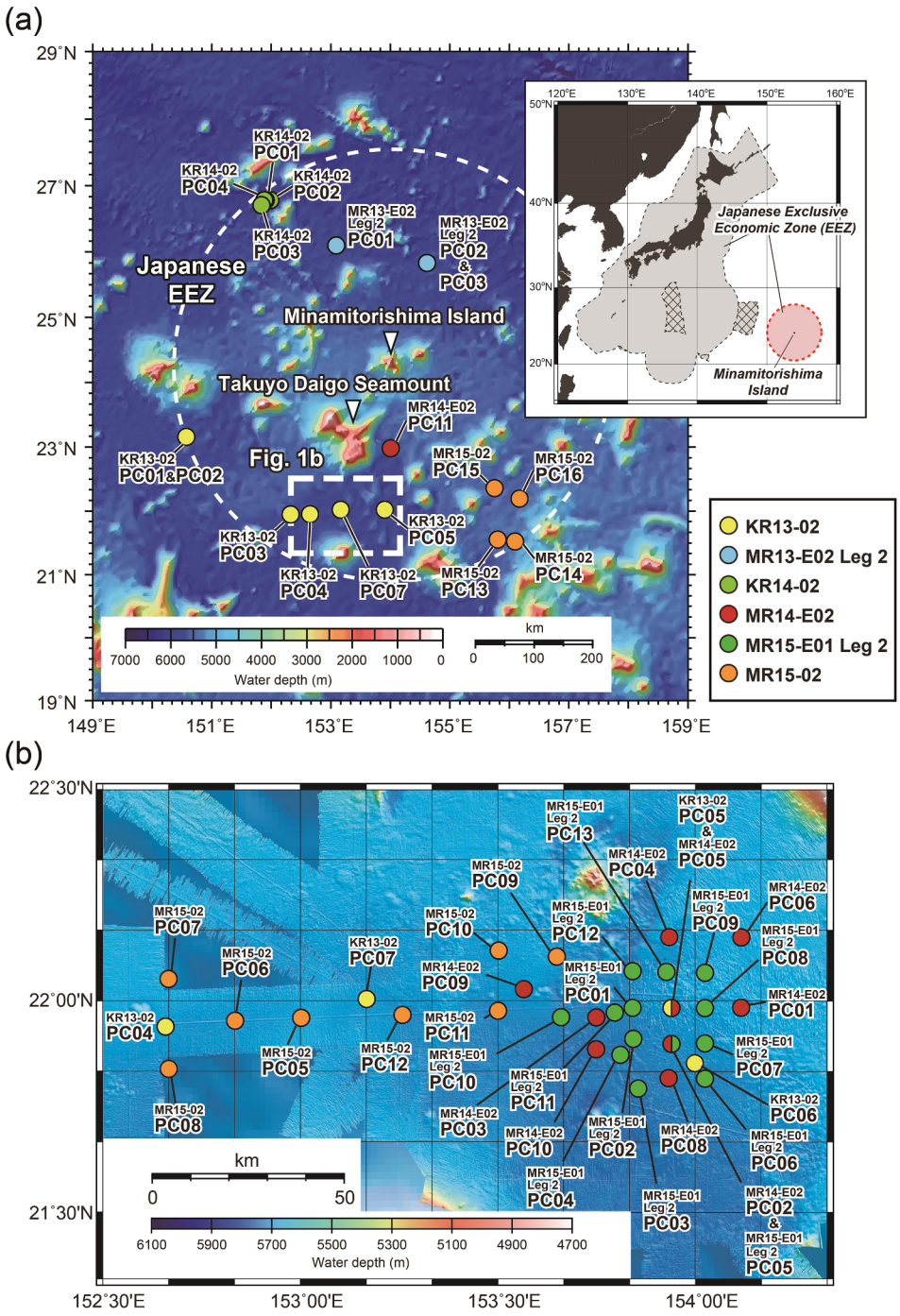

Fig. 1. Locations of the piston core sites and bathymetry within the Minamitorishima EEZ: (a) broad and (b) detailed maps. Hatched gray shading in Fig. 1a represents the extended continental shelves of Japan. Different research cruises are distinguished by color-coding. Bathymetric data for (a) are from ETOPO1 (NOAA National Centers for Environmental Information, NCEI; https://www.ngdc.noaa.gov/mgg/global/global.html). Bathymetric data for (b) are based on a compilation obtained during each research cruise mentioned in the text. The detailed sampling area indicated by the dashed rectangle in Fig. 1a is enlarged in Fig. 1b.

that individual BCP grains in REY-rich mud have maximum ΣREY values greater than 20000 ppm (Takaya et al., 2018). Owing to the remarkably high content of REY (especially of HREE), the extremely/highly REY-rich mud has attracted great attention as an unconventional and promising mineral resource for REY (Takaya et al., 2018; Yasukawa et al., 2018).

Noticeable peaks of REY content (including extremely and highly REY-rich mud) have been widely recognized in piston core samples recovered from the southern part of the Minamitorishima EEZ (Fujinaga et al., 2016; Iijima et al., 2016; Takaya et al., 2018). This finding suggests the existence of considerably REY-enriched layer(s) in this region. However, the depth profiles of ΣREY content of the piston core samples show no consistency in the depth, amplitude, and number of REY-enriched layers between cores (Figs. 2 and A.1). In addition, because the REY-rich mud has no visually distinctive features, a simple comparison of extremely/highly REY-rich mud layer(s) in different cores is difficult. As a result, the origin and distribution of these layers are still uncertain.

Under such circumstances, chemostratigraphy based on bulk geochemistry can provide new insights into the genesis of extremely REY-

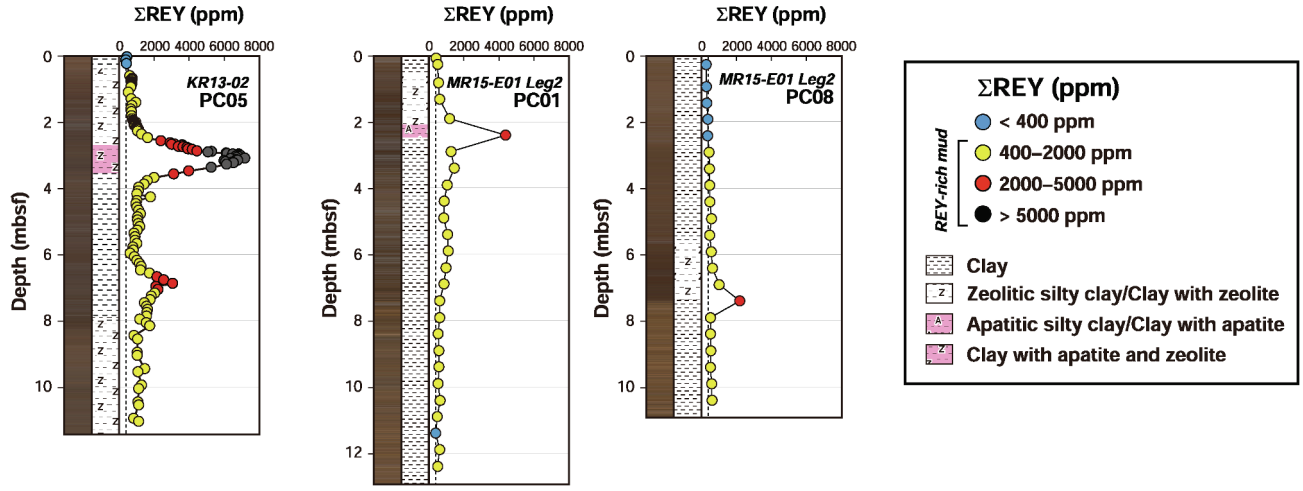

Fig. 2. Depth profiles of color, lithology, and ΣREY content of Cores KR13-02 PC05, MR15-E01 Leg2 PC01, and PC08. This figure includes data from Iijima et al. (2016), Takaya et al. (2018), and Yasukawa et al. (2018).

rich mud. Using this approach, we can characterize the sedimentary sequence of even apparently homogeneous sediments on the basis of subtle variations in the elemental compositions (Ratcliffe et al., 2010). In this study, we define the chemostratigraphy of the Minamitorishima sediments to clarify the stratigraphic positions and formation mechanism of the extremely/highly REY-rich mud layers.

2. Material and methods

2.1. Cruise information

The deep-sea sediment samples analyzed in this study were collected by piston corers during six research cruises (Cruises KR13-02, MR13-E02 Leg 2, KR14-02, MR14-E02, MR15-E01 Leg 2, and MR15-02) conducted by the Japan Agency of Marine-Earth Science and Technology (JAMSTEC) and the University of Tokyo within the Minamitorishima EEZ. Fujinaga et al. (2016) and Iijima et al. (2016) reported the details of Cruises KR13-02, MR13-E02 Leg 2, and KR14-02; here, we provide the details of three additional cruises (Cruises MR14-E02, MR15-E01 Leg 2, and MR15-02) conducted within the southern part of the Minamitorishima EEZ, where extremely REY-rich mud had previously been discovered.

Cruise MR14-E02 was conducted from 15 to 29 October 2014. During this cruise, 11 piston cores were collected. Cruises MR15-E01 Leg 2 and MR15-02 were conducted from 14 to 28 March and 22 June to 17 July 2015, respectively. Thirteen piston cores were obtained during Cruise MR15-E01 Leg 2 and 16 piston cores during Cruise MR15-02. All three of these cruises were carried out by *R/V Mirai* of JAMSTEC.

The sampling locations of the piston cores during these cruises are marked in Fig. 1, and the latitudes, longitudes, and water depths of the sites are listed in Table A.1. To investigate the spatial distribution of the extremely REY-rich mud, during Cruises MR14-E02 and MR15-E01 Leg 2, piston core samples were collected in a grid pattern centered on Core KR13-02 PC05 (Fig. 1b). In addition, an aim of Cruise MR15-02 was to investigate in detail the lateral continuity of the extremely/highly REY-rich mud along the east–west transect between Cores KR13-02 PC04 and PC05 (Fig. 1b).

2.2. Sediment samples

The lithostratigraphic schemes for each core in this study are illustrated in Figs. 2 and A.1. Sediment lithology was ascertained by means of on-board visual core descriptions and microscopic observations during each cruise, following the protocols of the International Ocean Discovery Program (IODP; Mazzullo et al., 1988; Ohta et al., 2016).

The main sediments in the Minamitorishima EEZ are brown, dark brown, and blackish-brown pelagic clay. They are in general composed of clay-sized particles, but several horizons contain a number of silt- to fine-sand-sized grains (more than 30% in smear slide observations; Ohta et al., 2016). The sediments in the northern part of the Minamitorishima EEZ are lighter in color and commonly contain many siliceous microfossils such as diatoms and radiolarians (Fujinaga et al., 2016). In the southern part of the Minamitorishima EEZ, sediments notably contain zeolite (phillipsite), ferromanganese micro-nodules and teeth/bone fragments of marine vertebrates that are collectively termed BCP (Iijima et al., 2016). Ohta et al. (2016), who analyzed the grain-size distribution of the constituent minerals of some representative cores, showed that the coarser (i.e. silt- to fine-sand-sized) grains are composed mainly of phillipsite and BCP, and that there is a larger proportion of coarser grains in the extremely/highly REY-rich mud. In addition, several cores contain lighter brown sediment at the deepest part of the sediment column. This sediment is associated with lighter and darker colored stripes, each a few centimeters thick. Some cores show clear lithological boundaries, whereas others show gradual changes in sediment color and lithology.

We collected sediment samples for chemical analyses with ~20 cm^3 scoops and sealed each sample in a small polyethylene bag on board.

2.3. Analytical methods

Bulk sediment samples were dried at 40 °C and pulverized to homogeneity with an agate pestle and mortar prior to the chemical analyses. After the powdered samples had been dried at 110 °C for 12 h, they were ignited at 950 °C for 6 h in a muffle furnace. Loss on ignition (LOI) was calculated from the weight lost by the samples. Following the LOI measurement, major-element contents were determined using a Rigaku ZSX Primus II X-ray fluorescence (XRF) spectrometer at the Frontier Research Center for Energy and Resources (FRCER)/Department of Systems Innovation, the University of Tokyo, Japan. The XRF analysis was conducted on glass beads made using 0.400 g of the ignited sample powder well mixed with 4.00 g of $Li_2B_4O_7$ flux (Merck Millipore Co. Spectromelt A10) and fused at 1190 °C for 7 min in a Pt crucible. Geochemical reference samples issued by the Geological Survey of Japan (GSJ) were used as calibration standards. The analytical results were within 3% (relative percentage difference) of accepted values for GSJ reference material JB-1b (Terashima et al., 1998). Details of the XRF analytical procedures were provided by Kato et al. (1998, 2002) and Yasukawa et al. (2014).

Trace-element and REY contents were determined by using

inductively coupled plasma mass spectrometers (an Agilent 7500c and a Thermo Fisher Scientific i-CAP Q) at the FRCER/Department of Systems Innovation, the University of Tokyo, following the procedures described by Kato et al. (2005) and Yasukawa et al. (2014). After drying at 110 °C for 12 h, another 0.050 g of the powdered sample split (without ignition) was completely decomposed by HNO_3–HF–$HClO_4$ digestion in a tightly sealed Teflon PFA (perfluoroalkoxy alkane) screw-cap beaker on a hot plate at 130 °C for 2 h. The digested sample was progressively evaporated at 110 °C for ~12 h, 160 °C for ~6 h, and 190 °C until dry. The residue was subsequently dissolved in 4.0 mL of HNO_3 and 1.0 mL of HCl, then the solution was diluted to 1:4000 by mass using Milli-Q water (18.2 MΩ·cm electrical resistivity at 25 °C). Spectral overlaps from oxides and hydroxides ($^{44}Ca^{16}O$ on ^{60}Ni, $^{47}Ti^{16}O$ on ^{63}Cu, $^{50}Ti^{16}O$ on ^{66}Zn, $^{135}Ba^{16}O$ and $^{134}Ba^{16}O^{1}H$ on ^{151}Eu, $^{137}Ba^{16}O$ and $^{136}Ba^{16}O^{1}H$ on ^{153}Eu, $^{141}Pr^{16}O$ and $^{140}Ce^{16}O^{1}H$ on ^{157}Gd, $^{143}Nd^{16}O$ on ^{159}Tb, and $^{165}Ho^{16}O$ on ^{181}Ta) were corrected following the method described by Aries et al. (2000). Analytical results of the GSJ reference materials JB-2 (Makishima and Nakamura, 2006) and JMS-2 (Takaya et al., 2014) typically yielded a relative percentage difference of < 5%.

3. Results

We used a compiled dataset of bulk major- and trace-element contents of the samples that were collected during the six cruises (Tables A.1 and A.2). The major-element data from Cruises MR15-E01 Leg 2 and MR15-02 and trace-element data from Cores MR15-02 PC05 to PC08 and PC12 to PC16 are newly reported in this paper; other results were documented elsewhere by Fujinaga et al. (2016), Iijima et al. (2016), Takaya et al. (2018), and Yasukawa et al. (2018, 2019).

Downhole variations of ΣREY contents of the studied cores are shown in Figs. 2 and A.1. A large number of the studied cores obtained from wide areas of the southern and southeastern part of the Minamitorishima EEZ show single or multiple layer(s) that have ΣREY contents greater than 2000 ppm (Figs. 2 and A.1). Here we define these layers as "REY peaks". This finding indicates that several layers of highly/extremely REY-rich mud are widely distributed in the studied area. However, the REY peaks differ in their amplitudes and occur at different depths below the seafloor in each core, even in adjacent cores within a distance of ~10 km (Figs. 1b, 2 and A.1). For example, we compare adjacent cores (KR13-02 PC05, MR15-E01 PC01, and PC08; Fig. 2) along an east–west transect: Core KR13-02 PC05 has double REY peaks at depths of 2.57–3.57 m below seafloor (mbsf) and 6.62–7.12 mbsf (Iijima et al., 2016); in contrast, Cores MR15-E01 PC01 and PC08 each have a single REY peak, at 2.14–2.64 mbsf and 7.15–7.65 mbsf, respectively. The highest value of each REY peak is also different between these cores (Figs. 1b and 2). As a consequence, the single REY peak in the latter two cores cannot be simply compared with either the upper or lower REY peak in the adjacent Core KR13-02 PC05. This difficulty has in turn hampered estimation of the distribution and elucidation of the formation timing and mechanism of the multiple REY peaks.

The bulk chemical compositions of the studied samples also display several distinctive data structures in some compositional subspaces (Fig. 3).

(1) In the Co–Ba diagram, there is a cluster of significantly Ba-enriched samples (up to ~1100 ppm), almost all of which contain less than ~120 ppm of Co (Fig. 3a). This sample group shows a negative correlation between Co and Ba contents, although the other samples exhibit a broadly positive correlation.
(2) In the scatter diagram of Co and TiO_2 contents (Fig. 3b), all data of the sediment samples form a circular structure.
(3) The CaO and P_2O_5 levels show a strong positive correlation (Fig. 3c), indicating that BCP grains significantly contribute to the chemical composition of bulk sediments (Fujinaga et al., 2016; Iijima et al., 2016). It should be noted that, in detail, there are two obvious parallel trends at CaO < 8 wt% and P_2O_5 < 5 wt% (Fig. 3c), which we refer to as the upper and lower trends.
(4) There is a strong positive correlation between ΣREY and P_2O_5 contents (Fig. 3d), indicating a contribution of REY-enriched BCP to bulk ΣREY contents. However, some samples with 2–7 wt% of P_2O_5 depart from the overall linear trend (Fig. 3d). This feature implies either enrichment of P_2O_5 or depletion of REY relative to the majority of the studied samples.
(5) In the TiO_2–Fe_2O_3* diagram (Fig. 3e), although most of the samples constitute a linear trend, a group with ~0.6 wt% of TiO_2 and ~7 wt % of Fe_2O_3* forms a minor but distinguishable data cluster deviating from the overall trend (Fig. 3e).

4. Discussion

4.1. Chemostratigraphic characterization

On the basis of the bulk chemical compositions of 1240 sediment samples from 49 cores within the Minamitorishima EEZ, we defined five chemostratigraphic units (Units I to V) in addition to the REY peaks.

Unit I: Sediments with ΣREY contents < 400 ppm can be classified into this unit. On the scatter diagram between Co and Ba (Fig. 4a), Unit I corresponds to the Ba-enriched samples that satisfy Ba (ppm) > Co + 330 (ppm). This unit constitutes the uppermost sediment in all cores collected within the Minamitorishima EEZ, except for four cores that lack this unit (Fig. 5).

Unit II: This unit is characterized by a high TiO_2 content (TiO_2 > 0.7 wt%; Fig. 4b) and more than 400 ppm of ΣREY (Fig. 4c). In almost all cores, this unit underlies Unit I (Fig. 6). It is noteworthy that the TiO_2 content clearly changes across the REY peak layer that is overlain by this unit (Fig. 6). Eight additional samples from the appropriate stratigraphic position were placed into Unit II, although the TiO_2 and ΣREY values of those samples are slightly lower than the definition given above (i.e., samples with TiO_2 = 0.65–0.70 wt% or ΣREY = 399–400 ppm; Table A.3).

Unit III: This unit is characterized by notably high Fe_2O_3*/TiO_2 values (Fig. 4d), and occurs under Unit II (Figs. 5 and 6). In Fig. 4d, a minor cluster (purple symbols in Fig. 4) can be separated from the overall trend by a line with a slope of Fe_2O_3*/TiO_2 = 11 as an arbitrarily assigned threshold. The samples in the minor cluster are categorized into this unit. An additional 12 samples with Fe_2O_3*/TiO_2 slightly lower than 11 (Fe_2O_3*/TiO_2 = 10.3–10.9; Table A.3) were also assigned to Unit III. These 12 samples constitute 8% of the 149 samples that were finally categorized into Unit III.

Units IV and V: All of the remaining samples occur in the lowermost part of the sediment column of the Minamitorishima EEZ. These samples can be further classified into two units on the basis of their P_2O_5/ΣREY values. Samples characterized by significantly high P_2O_5/ΣREY values (P_2O_5/ΣREY > 0.0018; Fig. 4c) are categorized as Unit IV. These samples are shown in yellow in the P_2O_5–ΣREY diagram (Fig. 4c) and deviate from the major linear trend. The remaining samples are classified into Unit V, which is intercalated within Unit IV (Figs. 5 and 6).

4.2. Causes of the chemical characteristics of the chemostratigraphic units

The most obvious feature of Unit I is its low ΣREY content compared to the other units (Fig. 7). The post-Archean Australian shale (PAAS)-normalized REY patterns of this unit are almost flat and show similar elemental abundances to those of PAAS (Fig. 7), implying that Unit I is mainly composed of terrigenous material. This result is consistent with the results of Yasukawa et al. (2019), who demonstrated a contribution of detrital components from the Taklimakan Desert–Chinese loess plateau to the non-REY-rich Minamitorishima sediments on the basis of Pb, Sr, and Nd isotopic ratios. Indeed, continental detrital materials

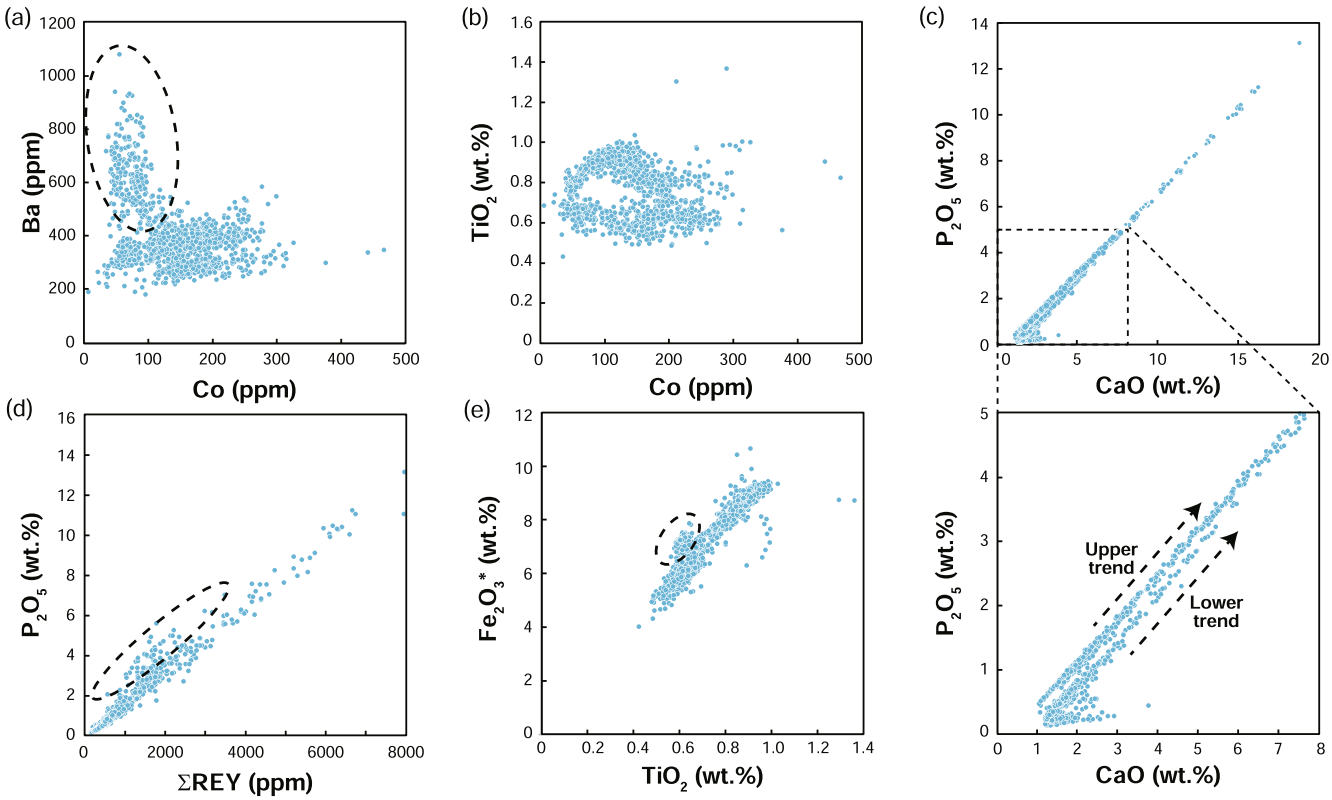

Fig. 3. Representative scatter diagrams of the chemical compositions of the Minamitorishima sediment samples: (a) Co vs Ba, where the dashed ellipse encloses samples enriched in Ba compared to Co; (b) Co vs TiO_2; (c) CaO vs P_2O_5 (the outset plot shows an enlarged view of samples with < 8 wt% CaO and < 5 wt% P_2O_5); (d) ΣREY vs P_2O_5, where the dashed ellipse indicates the samples that depart from the overall linear trend; and (e) TiO_2 vs Fe_2O_3* (total Fe as Fe_2O_3), where the dashed ellipse indicates the samples that deviate from the overall trend.

typically contain > 600 ppm Ba (Plank and Langmuir, 1998; Rudnick and Gao, 2014). In addition, this unit contains relatively abundant siliceous microfossils (Fujinaga et al., 2016), consistent with enrichment of biogenic Ba and thus a relatively high bulk Ba content in the sediment of Unit I (Fig. 4a; Plank and Langmuir, 1998). Consequently, the low ΣREY content of this unit can be attributed to dilution by terrigenous and biogenic components.

The Co content in pelagic clay is generally controlled by a slowly depositing hydrogenous component and thus increases under low sedimentation rates (Zhou and Kyte, 1992). Considering this point, the negative correlation of Ba and Co in Unit I reflects the dilution of Co by continental detrital materials with relatively lower Co contents (~17 ppm; Rudnick and Gao, 2014), which deposit at a higher sedimentation rate than typical pelagic clay. On the other hand, the positive correlation of Ba and Co in Units II–V indicates the slow and constant deposition of Ba and hydrogenous Co. Such slow Ba deposition might result from low primary productivity, and thus reduced production of biogenic Ba (Plank and Langmuir, 1998; Paytan et al., 1998), in the oligotrophic ocean where pelagic clay is deposited.

The sediments in Units I and II are characterized by TiO_2 > 0.7 wt % (Fig. 4b), whereas those in Units III, IV, and V contain < 0.7 wt% of TiO_2. Notably, the sediments in the high-Ti units (Units I and II, or the upper part of the sediment column) also constitute the lower trend in the CaO–P_2O_5 diagram, whereas those in the low-Ti units (Units III to V, or the lower part of the sediment column) constitute the upper trend (Figs. 3c and 4e). In addition, the upper and lower trends converge with increasing CaO and P_2O_5 contents. Given that the linear trend between CaO and P_2O_5 contents indicates a mixing relationship between BCP and terrigenous matrix, the two trends may represent a shift in the terrigenous end members (i.e., intercepts of the trends) of different chemical compositions, rather than variable BCP chemical compositions (e.g., hydroxyapatite, fluorapatite, chlorapatite). Therefore, these geochemical characteristics likely reflect a change in the provenance of terrigenous components between Units II and III.

High Fe/Ti ratios are characteristic of Unit III. As discussed above, the TiO_2 content of Unit III is comparable to those of Units IV and V; thus, the high Fe/Ti ratios in this unit indicate its relative enrichment in Fe (Fig. 4d). Moreover, in the CaO–P_2O_5 diagram, Unit III constitutes the upper trend together with Units IV and V (Fig. 4e). This result indicates that the Fe enrichment in Unit III cannot be attributed to a difference in terrigenous components between Unit III and Units IV and V. One possible explanation for the excess Fe is hydrothermal activity; however, considering that the Minamitorishima EEZ was located far from the East Pacific Rise (EPR) even when the underlying Cretaceous chert was deposited (Lancelot and Larson, 1990; Yasukawa et al., 2019), this Fe excess is unlikely to have been caused by hydrothermal input. Another possible explanation is the influence of a hydrogenous component (Hein et al., 2013). Indeed, Unit III is characterized by high Mn and Co contents (Fig. 4f), which are known to be enriched in Fe–Mn (oxyhydr)oxides of hydrogenous origin. Therefore, the high Fe/Ti ratio of Unit III likely resulted from the influence of hydrogenous Fe–Mn (oxyhydr)oxides.

The deviation of the Unit IV samples from the major linear trend of all other samples is apparent in the scatter diagram of P_2O_5 and ΣREY (Fig. 4c). In the CaO–P_2O_5 diagram, however, the Unit IV samples do not deviate from the upper mixing trend between a terrigenous component and BCP (Fig. 4e). This result suggests that the relatively high P_2O_5/ΣREY ratios of the Unit IV samples did not result from a relatively high ΣREY content of the terrigenous component and/or BCP, but from the relatively low ΣREY content of the BCP in this unit.

4.3. Stratigraphic position and lateral extent of REY peaks

The chemostratigraphic positions of the REY peaks in the 49 piston

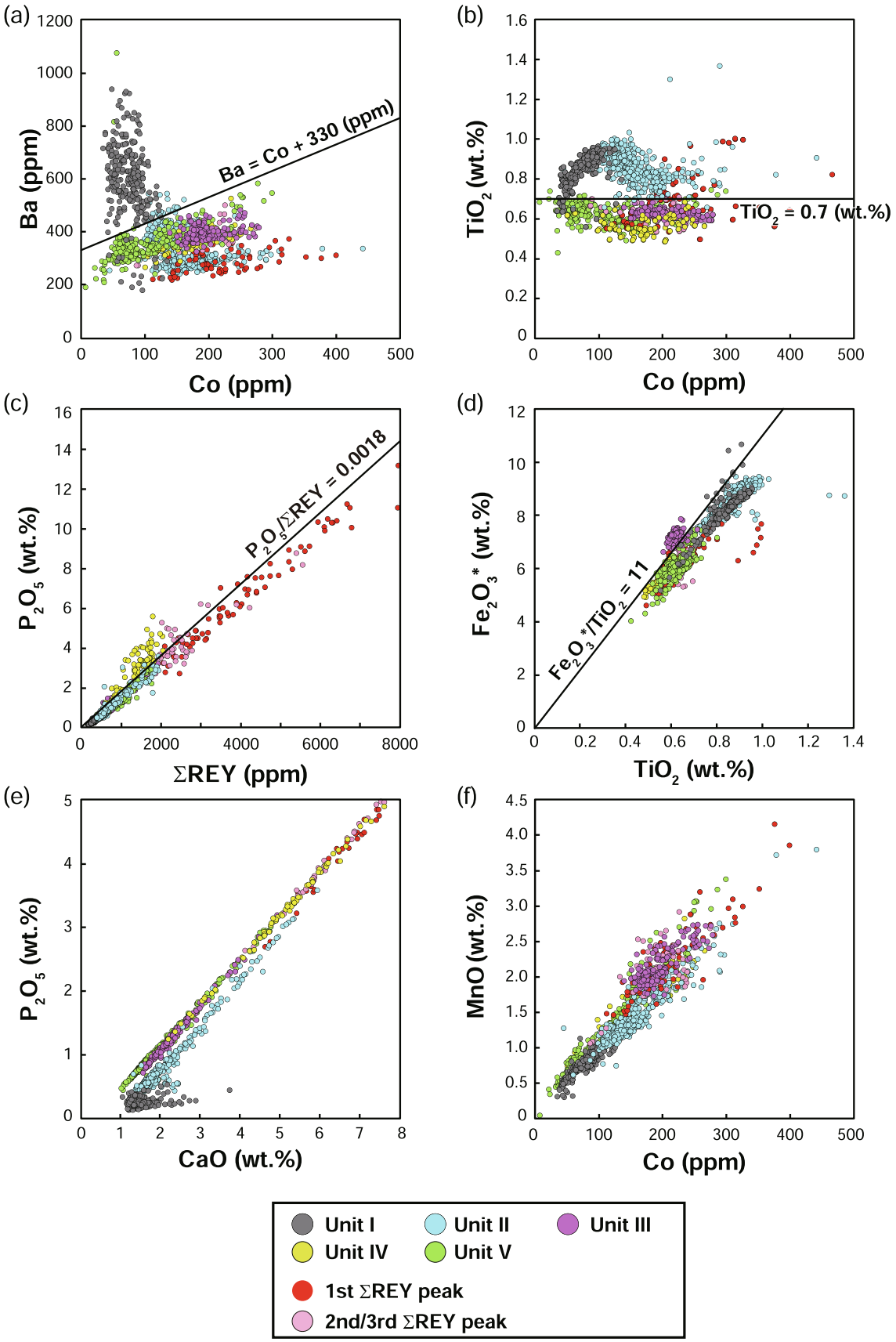

Fig. 4. Representative scatter diagrams of sample data color-coded on the basis of the chemostratigraphic scheme constructed in this study (Section 4.1): (a) Co vs Ba, (b) Co vs TiO_2, (c) ΣREY vs P_2O_5, (d) TiO_2 vs Fe_2O_3*, (e) CaO vs P_2O_5 (enlarged view of samples with < 8 wt% CaO and < 5 wt% P_2O_5), and (f) Co vs MnO. Solid black lines denote the thresholds characterizing each sediment unit (Section 4.1). It should be noted that P_2O_5/ΣREY values are reported in wt.%/ppm. Fe_2O_3* indicates total iron as Fe_2O_3, measured by XRF analysis.

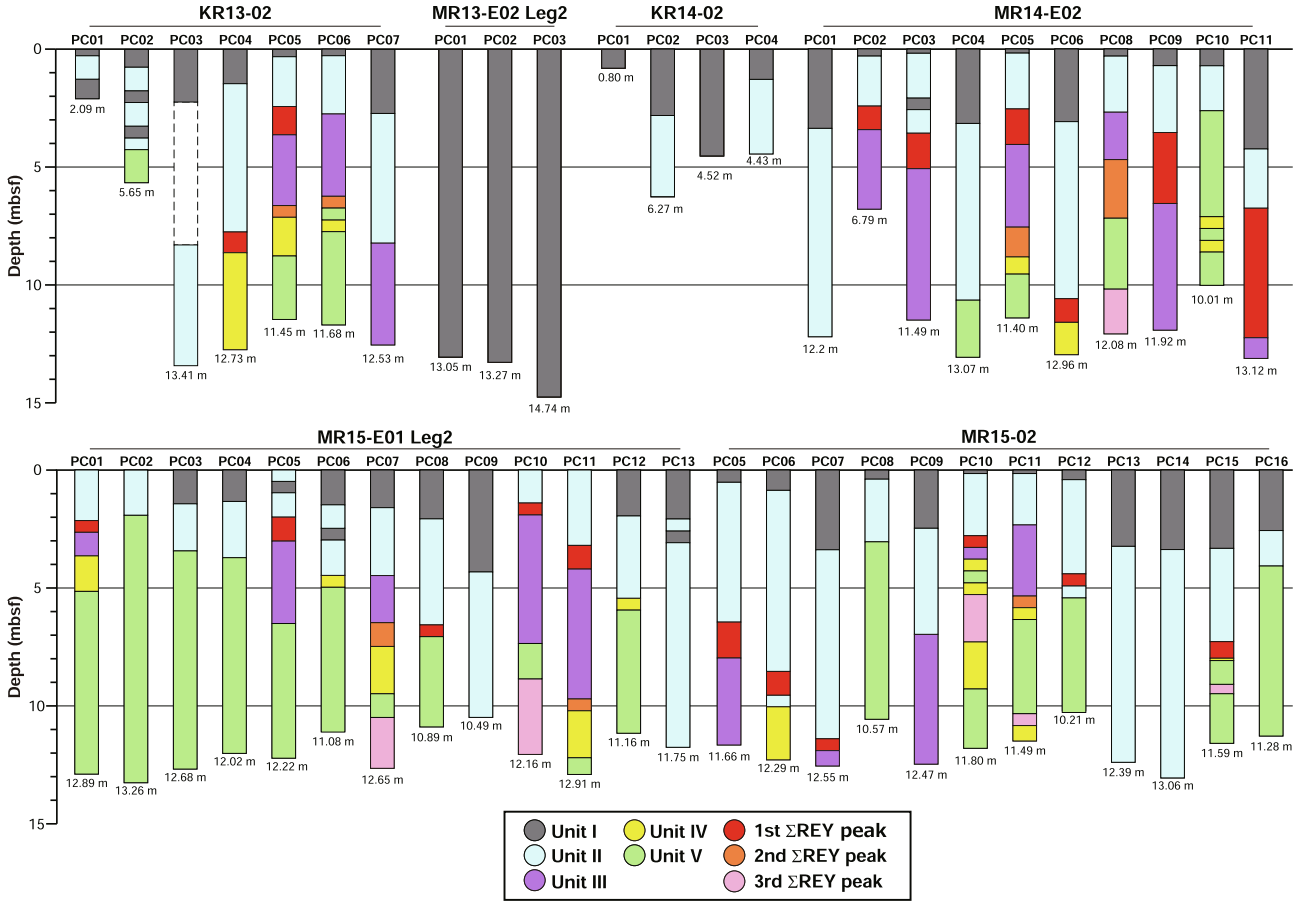

Fig. 5. Chemostratigraphic classification of all cores used in this study.

cores are shown in Fig. 5. In many cores, a REY peak is present just below Unit II, although a few cores also exhibit REY peaks just below Unit III and/or within Units IV and V. This pattern suggests that at least three REY peaks are distinguishable on the basis of chemostratigraphy even in the visually homogenous pelagic sediments. We term these REY peaks the "*1st REY peak*" below Unit II, the "*2nd REY peak*" below Unit III, and the "*3rd REY peak*" intercalated within Units IV and V, downward from the seafloor surface.

By applying the chemostratigraphy, the *1st REY peak* can be identified in most of the cores in the southern part of the Minamitorishima EEZ, as shown in Fig. 8. This finding indicates a wide distribution of the *1st REY peak* in the southern part of the Minamitorishima EEZ. The chemostratigraphy also revealed that the depth of the *1st REY peak* is dependent on the thicknesses of Units I and II (Fig. 8).

The east–west transect of the southern part of the Minamitorishima EEZ (Fig. 8a) shows a clear trend that Units I and II are thinner (< 5 m) in the central part of the east–west transect (from Core KR13-02 PC05 to Core MR15-02 PC11) and become thicker (~10 m) at the western and eastern ends (from Core MR14-E02 PC01 to Core MR15-01 PC08 and from Core KR13-02 PC07 to Core KR13-02 PC04, respectively). In particular, Cores MR15-E01 PC01, PC10, and PC11 do not contain Unit I, resulting in the shallowest depth of the *1st REY peak*. A similar trend can also be seen in the north–south transect (Fig. 8b); the three southern cores contain thinner Units I and II, and those units are thicker in the other cores.

In contrast to the *1st REY peak*, the *2nd* and *3rd REY peaks* occur in fewer cores (Fig. 5). In the east–west and north–south transects (Fig. 8), the *2nd* and *3rd REY peaks* are recognizable in only five and three cores, respectively. This finding suggests that the *2nd* and *3rd REY peaks* are not widely distributed in this area, as in the case of the *1st REY peak*.

4.4. Cause of the absence of units and REY peaks

The chemostratigraphy also shows that a significant number of the studied cores do not contain all the units below the *1st REY peak* (Units III to V as well as the *2nd* and *3rd REY peaks*), even though almost all cores contain Units I and II (Figs. 5 and 6). In the east–west transect (Fig. 8a), for example, Cores KR13-02 PC05 and MR15-E01 PC11 contain all chemostratigraphic units except for the *3rd REY peak*. However, Core MR15-E01 PC08 has only Unit I, Unit II, the *1st REY peak*, and Unit V, although this core is located adjacent to Core KR13-02 PC05. This result indicates that Core MR15-E01 PC08 lacks Units III to IV, the *2nd REY peak*, and the *3rd REY peak*. Similarly, Cores KR13-02 PC04 and MR15-02 PC06, which are situated in the western part of the east–west transect, lack Unit III and the *2nd* and *3rd REY peaks*; thus, the *1st REY peak* in these cores occurs just above Unit IV. Moreover, Cores KR13-02 PC07 and MR15-02 PC11, in the central part of the east–west transect, lack only the *1st REY peak*. In the north–south transect, Core MR14-E02 PC04 contains only Units I, II, and V, and lacks the *1st REY peak*, Units III and IV, the *2nd REY peak*, and the *3rd REY peak* (Fig. 8b). In addition, MR15-E01 PC05 lacks the *2nd* and *3rd REY peaks* and Unit IV, and the southernmost core, MR14-02 PC08, lacks Unit IV as well as the *1st REY peak*.

There are two possible reasons for the absence of units and REY peaks: (1) piston cores cannot reach the depths of lower units and REY peaks or (2) the units and REY peaks are actually absent as a result of physical processes such as hiatuses or erosion. Possibility (1) can be assessed by considering the sub-bottom profiler (SBP) data from the Minamitorishima EEZ (Nakamura et al., 2016). It is obvious that the piston cores used in this study penetrated at most half of the total depth from the seafloor to the acoustic basement (which probably consists of chert). Therefore, in the cores containing only the upper units, the

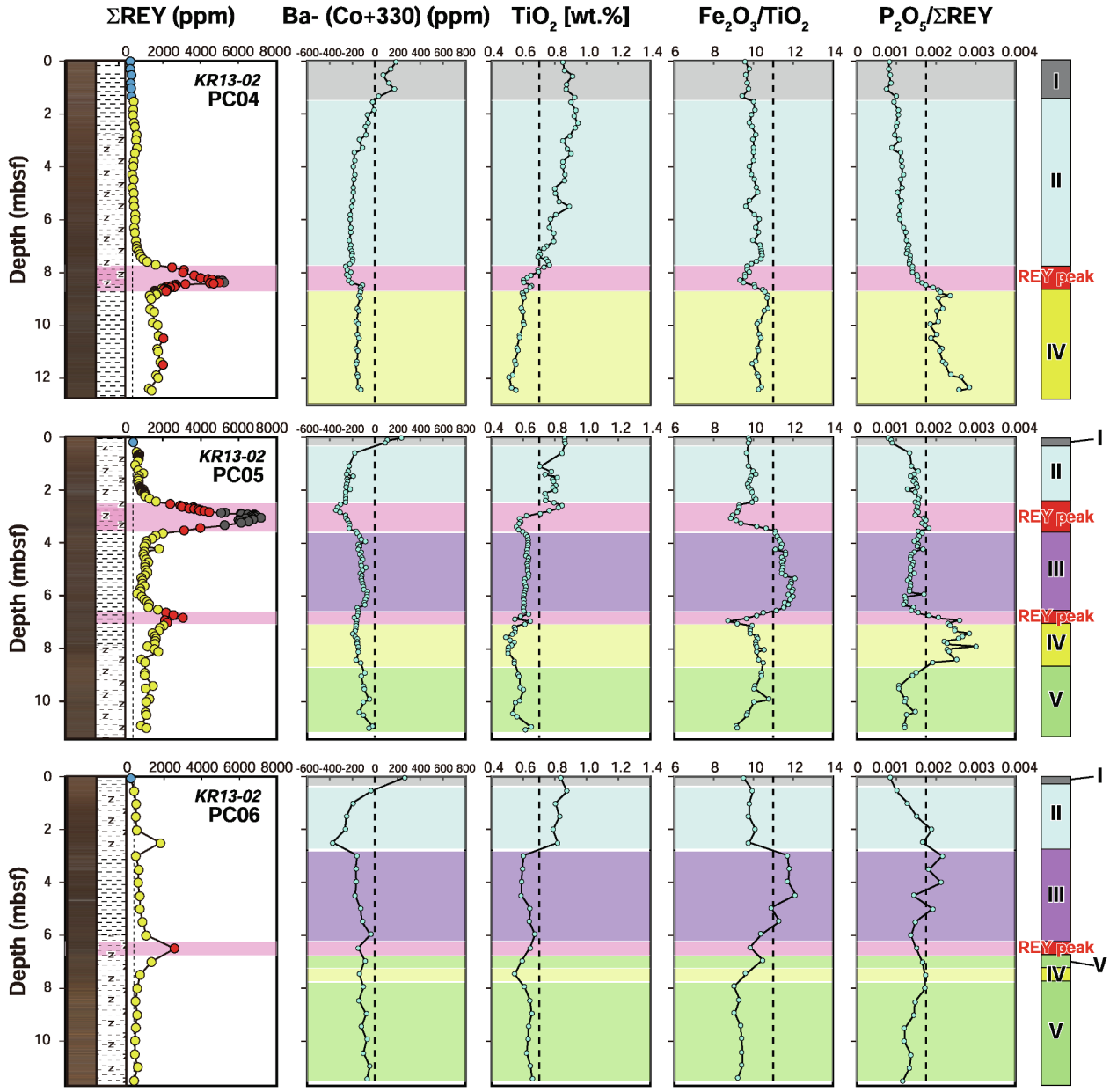

Fig. 6. Representative depth profiles of geochemical indices characterizing the chemostratigraphy in Cores KR13-02 PC04, PC05, and PC06: Ba – (Co + 330) [ppm], TiO_2 [wt.%], Fe_2O_3*/TiO_2, and P_2O_5/ΣREY [wt.%/ppm]. Vertical dashed lines indicate the threshold values detailed in Section 4.1 (see Fig. 4). For comparison, ΣREY profiles are also shown. The colored boxes in the background correspond to the color-coding of each chemostratigraphic unit in Figs. 4 and 5.

lower units and/or REY peaks may be present in the deeper part that has not yet been investigated. However, some cores reaching to Unit V (the lowermost unit of the sediment column) obviously lack Unit III, Unit IV, the *2nd REY peak*, and/or the *3rd REY peak*. This observation indicates that possibility (1) alone cannot explain the absence of the units and REY peaks.

Concerning possibility (2), the absence of one or more chemostratigraphic units immediately below the *1st REY peak* indicates that a hiatus or erosion occurred prior to or during the formation of the REY peak. Variable numbers of units and variable missing thicknesses (as much as several meters of sediment) occur in a relatively small area, forming obvious unconformities (e.g., between Units II and V in Core MR15-E01 Leg 2 PC04; Fig. 9). This feature implies that a hiatus (i.e., cessation of sediment deposition) is unrealistic for the absence of the units and REY peaks; instead, physical erosion of the sediments on a local scale appears to be a more plausible mechanism to explain the observation. A possible process for such significant physical erosion of pelagic sediment is the enhancement of bottom currents, which has long been cited as a mechanism that inhibits continuous deposition, causes sedimentary erosion, and results in disconformities within sedimentary sequences (Keller and Barron, 1987; Kennett and Watkins, 1975, 1976; Zhou and Kyte, 1992). It is worth noting that 16 cores lack the *1st REY peak* (Cores KR13-02 PC02, PC06, PC07, MR14-E02 PC04, PC08, PC10, MR15-E01 PC02, PC03, PC04, PC06, PC07, PC12, MR15-02 PC08, PC09, PC11, and PC16; Figs. 5 and 8). This result indicates that the erosion occurred during the formation of the *1st REY peak*. The erosion can be considered to have caused the absence of one or more units below the *1st REY peak*, including the *2nd* and *3rd REY peaks*, which in turn resulted in the local and discontinuous distribution of the *2nd* and *3rd REY peaks*. In addition, the *2nd* and *3rd REY peaks* in some cores are underlain by Unit IV, whereas they directly overlie Unit V in other cores. This result leads us to consider that erosion also occurred during the formation of the *2nd* and *3rd REY peaks*.

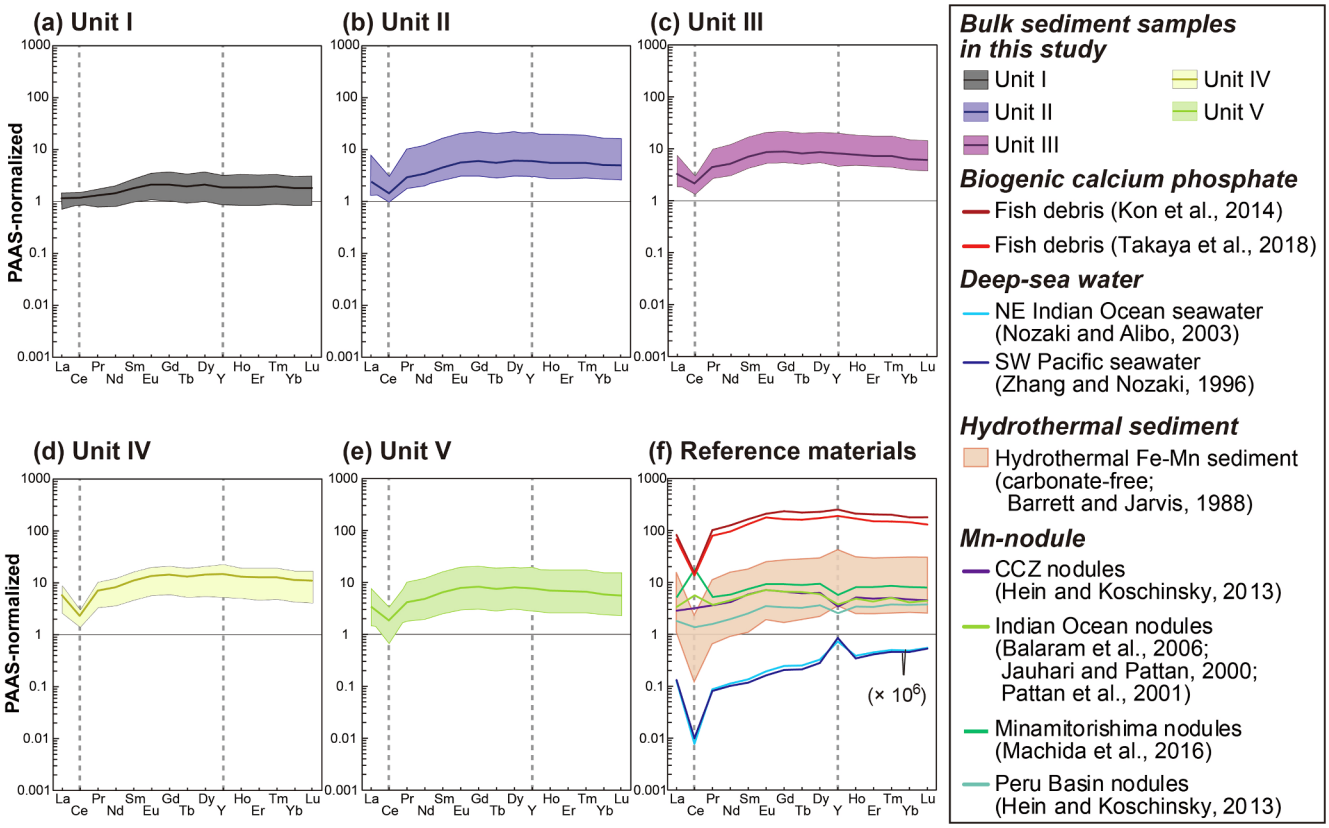

Fig. 7. PAAS-normalized REY patterns of (a)–(e) sample data of Units I to V and (f) reference materials. In (a) to (e), the colored lines and shaded areas indicate the averages and ranges, respectively, of the PAAS-normalized values of each unit. The PAAS data are from (Taylor and McLennan, 1985). The data sources of the reference materials are as follows. Biogenic calcium phosphate: (Kon et al., 2014; Takaya et al., 2018). Deep-sea water: (Nozaki and Alibo, 2003; Zhang and Nozaki, 1996). Hydrothermal sediment: (Barrett and Jarvis, 1988). Mn-nodule: (Hein and Koschinsky, 2013; Jauhari and Pattan, 2000; Machida et al., 2016; Pattan et al., 2001).

4.5. Implications for formation of the REY peaks

Ohta et al. (2016) suggested that enhancement of bottom currents can produce selective accumulation of coarse BCP grains enriched in REY, resulting in the formation of the prominent REY peaks in the Minamitorishima EEZ. Our observations provide important evidence to support the mechanism proposed by Ohta et al. (2016). However, it should be noted that if the bottom current was sufficiently strong during deposition of the REY peaks, the current could have hampered the accumulation of BCP grains or even eroded the sediment as a whole. The magnitude of the erosion may have been affected by local conditions, resulting in deposition of locally variable amounts of sedimentary load, including BCP. This process can explain the large variations in thickness, stratigraphic positions, and ΣREY contents of the REY peaks, even in adjacent cores.

The SBP survey in the Minamitorishima EEZ revealed that Unit I is variable in thickness or absent at some locations, especially in the southern and southeastern parts of the EEZ (Nakamura et al., 2016). Our results confirm this thickness variation and, in some cores, the absence of Unit I as discussed in Section 4.4 (Fig. 8). The absence of the uppermost layers of the sediment column strongly suggests recent or ongoing erosion in this area. We note, however, that no REY peak was detected in Units I and II, above the *1st REY peak*. This observation indicates the possibility that some process(es) other than sorting of BCP by a strong bottom current additionally contributed to the formation of the REY peaks.

5. Conclusions

Our investigation of a comprehensive geochemical dataset of 1240 samples from 49 cores in the Minamitorishima EEZ yielded the following conclusions.

1. Deep-sea sediments within the Minamitorishima EEZ can be classified into five chemostratigraphic units and REY peaks on the basis of their geochemical features in multi-elemental compositional space.
2. The chemostratigraphic scheme revealed that REY peaks occur in three stratigraphic positions within the sediment column: (1) just below Unit II, (2) just below Unit III, or (3) intercalated within Units IV and V. These are termed the *1st, 2nd*, and *3rd REY peaks*, respectively. The *1st REY peak* is continuously distributed throughout the southern to southeastern part of the Minamitorishima EEZ, and the depth of its occurrence is controlled simply by the thickness of Units I and II. In contrast, the *2nd* and *3rd REY peaks* appear in a more limited number of cores.
3. The variable pattern of sediment loss just below or concurrent with the REY peaks indicates that erosion events occurred during the deposition of REY peaks. This, in turn, suggests a causal relationship between sediment erosion and the formation of REY peaks (including extremely/highly REY-rich mud layers).
4. The thinning or absence of Units I and II indicates the occurrence of very recent or ongoing erosion in the Minamitorishima EEZ. However, there is no REY peak in the sediment layers above the *1st REY peak*. This result strongly suggests that other geological factor (s) in addition to physical erosion might have played a significant role in the extreme REY enrichment on the deep seafloor.

Declaration of Competing Interest

The authors declare that they have no known competing financial

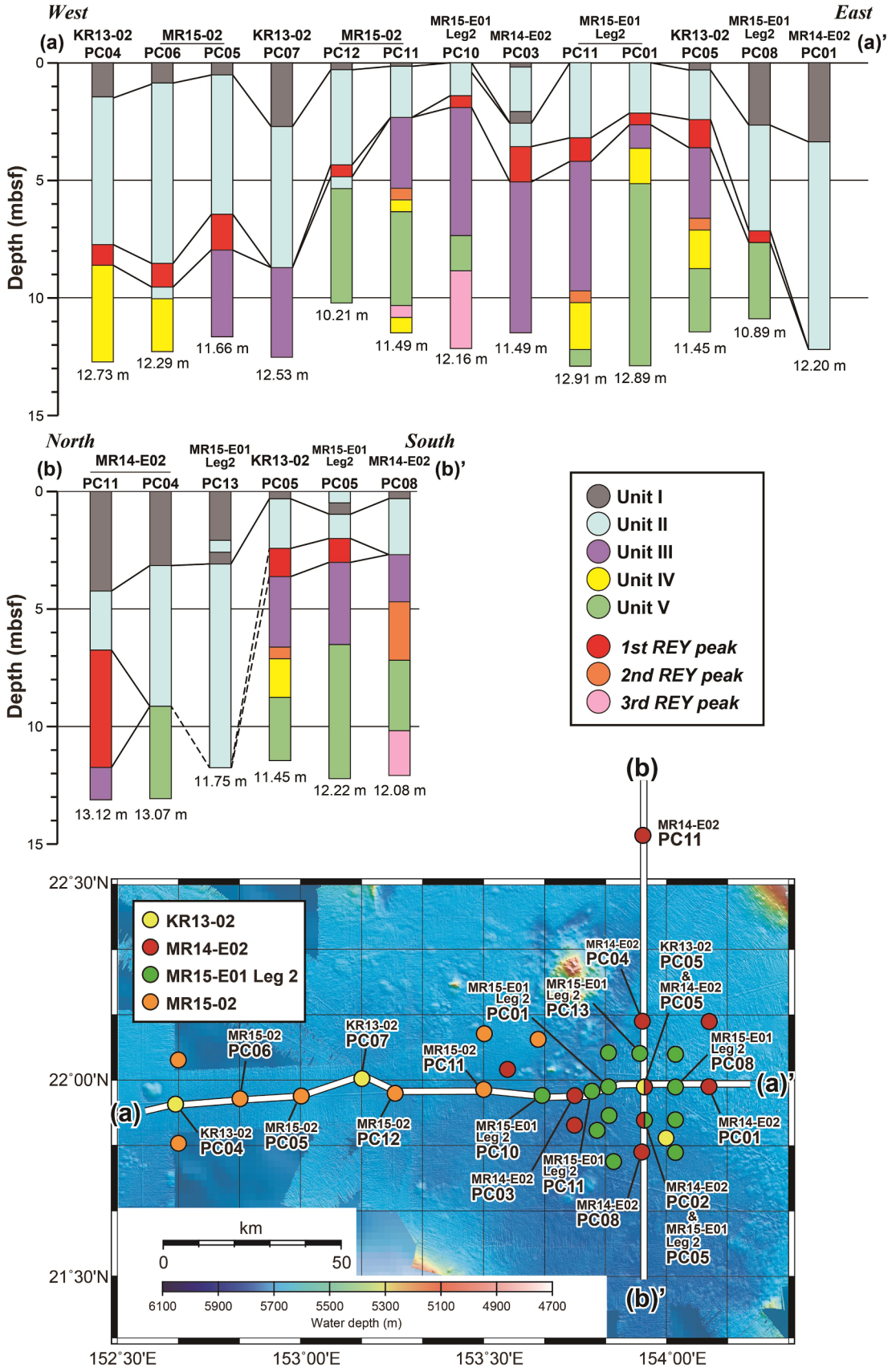

Fig. 8. Chemostratigraphic correlation along representative east–west (a–a') and north–south (b–b') transects of the studied sites, both of which include Core KR13-02 PC05 as a benchmark. It is remarkable that Core KR13-02 PC05 contains almost all types of sediments defined in our chemostratigraphy, except for the *3rd REY peak*.

Fig. 9. Photograph of Core MR15-E01 Leg 2 PC04. An obvious unconformity corresponding to the boundary between Unit II and Unit V is present in the middle of Sec. 04 (white arrow).

interests or personal relationships that could have appeared to influence the work reported in this paper.

Acknowledgements

We thank the shipboard scientific parties and crews of R/Vs Kairei and Mirai for their dedicated work. We are grateful to Y. Itabashi and C. Kabashima for their assistance with the chemical analyses. This research was financially supported by Japan Society for the Promotion of Science (JSPS) KAKENHI Grants No. JP15H05771 to Y.K., No. JP25289334 and No. JP17H01361 to N.K., No. JP18K14168 to K.Y. and No. JP18J22633 to E.T.

Appendix A. Supplementary data

Supplementary data to this article can be found online at https://doi.org/10.1016/j.oregeorev.2020.103392.

References

Aries, S., Valladon, M., Polvé, M., Dupré, B., 2000. A routine method for oxide and hydroxide interference corrections in ICP-MS chemical analysis of environmental and geological samples. Geostand. Newsl. 24, 19–31. https://doi.org/10.1111/j.1751-908X.2000.tb00583.x.

Arrhenius, G., Bramlette, M.N., Picciotto, E., 1957. Localization of radioactive and stable heavy nuclides in ocean sediments. Nature 180, 85–86. https://doi.org/10.1038/180085a0.

Barrett, T.J., Jarvis, I., 1988. Rare-earth element geochemistry of metalliferous sediments from DSDP Leg 92: The East Pacific Rise transect. Chem. Geol. 67, 243–259. https://doi.org/10.1016/0009-2541(88)90131-3.

Bernat, M., 1975. Les isotopes de l'uranium et du thorium et les terres rares dans l'environnement marin. Cah. O.R.S.T.O.M. série Géologie 7, 65–83.

Fujinaga, K., Yasukawa, K., Nakamura, K., Machida, S., Takaya, Y., Ohta, J., Araki, S., Liu, H., Usami, R., Maki, R., Haraguchi, S., Nishio, Y., Usui, Y., Nozaki, T., Yamazaki, T., Ichiyama, Y., Ijiri, A., Inagaki, F., Machiyama, H., Iijima, K., Suzuki, K., Kato, Y., 2016. Geochemistry of REY-rich mud in the Japanese exclusive economic zone around Minamitorishima island. Geochem. J. 50, 575–590. https://doi.org/10.2343/geochemj.2.0432.

Hein, J.R., Koschinsky, A., 2013. Deep-Ocean Ferromanganese Crusts and Nodules. In: Treatise on Geochemistry, Second Edition. Elsevier, pp. 273–291. https://doi.org/10.1016/B978-0-08-095975-7.01111-6.

Hein, J.R., Mizell, K., Koschinsky, A., Conrad, T.A., 2013. Deep-ocean mineral deposits as a source of critical metals for high- and green-technology applications: Comparison with land-based resources. Ore Geol. Rev. 51, 1–14. https://doi.org/10.1016/j.oregeorev.2012.12.001.

Iijima, K., Yasukawa, K., Fujinaga, K., Nakamura, K., Machida, S., Takaya, Y., Ohta, J., Haraguchi, S., Nishio, Y., Usui, Y., Nozaki, T., Yamazaki, T., Ichiyama, Y., Ijiri, A., Inagaki, F., Machiyama, H., Suzuki, K., Kato, Y., 2016. Discovery of extremely REY-rich mud in the western North Pacific Ocean. Geochem. J. 50, 557–573. https://doi.org/10.2343/geochemj.2.0431.

Jauhari, P., Pattan, J.N., 2000. Ferromanganese nodules from the Central Indian Ocean Basin. In: Cronan, D.S. (Ed.), Handbook of Marine Mineral Deposits. CRC Press, Boca Raton, Florida, pp. 171–195.

Kashiwabara, T., Toda, R., Fujinaga, K., Honma, T., Takahashi, Y., Kato, Y., 2014. Determination of host phase of Lanthanum in deep-sea REY-rich mud by XAFS and μ-XRF Using high-energy synchrotron radiation. Chem. Lett. 43, 199–200. https://doi.org/10.1246/cl.130853.

Kashiwabara, T., Toda, R., Nakamura, K., Yasukawa, K., Fujinaga, K., Kubo, S., Nozaki, T., Takahashi, Y., Suzuki, K., Kato, Y., 2018. Synchrotron X-ray spectroscopic perspective on the formation mechanism of REY-rich muds in the Pacific Ocean. Geochim. Cosmochim. Acta 240, 274–292. https://doi.org/10.1016/j.gca.2018.08.013.

Kato, Y., Fujinaga, K., Nakamura, K., Takaya, Y., Kitamura, K., Ohta, J., Toda, R., Nakashima, T., Iwamori, H., 2011. Deep-sea mud in the Pacific Ocean as a potential resource for rare-earth elements. Nat. Geosci. 4, 535–539. https://doi.org/10.1038/ngeo1185.

Kato, Y., Fujinaga, K., Suzuki, K., 2005. Major and trace element geochemistry and Os isotopic composition of metalliferous umbers from the Late Cretaceous Japanese accretionary complex: COMPOSITION OF METALLIFEROUS UMBERS. Geochem. Geophys. Geosyst. 6 (7).

Kato, Y., Nakao, K., Isozaki, Y., 2002. Geochemistry of Late Permian to Early Triassic pelagic cherts from southwest Japan: implications for an oceanic redox change. Chem. Geol. 182, 15–34. https://doi.org/10.1016/S0009-2541(01)00273-X.

Kato, Y., Ohta, I., Tsunematsu, T., Watanabe, Y., Isozaki, Y., Maruyama, S., Imai, N., 1998. Rare earth element variations in mid-Archean banded iron formations: implications for the chemistry of ocean and continent and plate tectonics. Geochim. Cosmochim. Acta 62, 3475–3497. https://doi.org/10.1016/S0016-7037(98)00253-1.

Keller, G., Barron, J.A., 1987. Paleodepth distribution of Neocene deep-sea hiatuses. Paleoceanography 2, 697–713. https://doi.org/10.1029/PA002i006p00697.

Kennett, J.P., Watkins, N.D., 1975. Deep-sea erosion and manganese nodule development in the southeast indian ocean. Science (80-.) 188, 1011–1013. https://doi.org/10.1126/science.188.4192.1011.

Kennett, J.P., Watkins, N.D., 1976. Regional deep-sea dynamic processes recorded by late Cenozoic sediments of the southeastern Indian Ocean. Geol. Soc. Am. Bull. 87, 321. https://doi.org/10.1130/0016-7606(1976) 87<321:RDDPRB>2.0.CO;2.

Kon, Y., Hoshino, M., Sanematsu, K., Morita, S., Tsunematsu, M., Okamoto, N., Yano, N., Tanaka, M., Takagi, T., 2014. Geochemical Characteristics of Apatite in Heavy REE-rich Deep-Sea Mud from Minami-Torishima Area Southeastern Japan. Resour. Geol. 64, 47–57. https://doi.org/10.1111/rge.12026.

Lancelot, Y., Larson, L., 1990. Site 800, in: Proceedings of the Ocean Drilling Program, 129 Initial Reports. Ocean Drilling Program, pp. 33–89. https://doi.org/10.2973/odp.proc.ir.129.102.1990.

Machida, S., Fujinaga, K., Ishii, T., Nakamura, K., Hirano, N., Kato, Y., 2016. Geology and geochemistry of ferromanganese nodules in the Japanese Exclusive Economic Zone around Minamitorishima Island. Geochem. J. 50, 539–555. https://doi.org/10.2343/geochemj.2.0419.

Makishima, A., Nakamura, E., 2006. Determination of major/minor and trace elements in silicate samples by ICP-QMS and ICP-SFMS applying isotope dilution-internal standardisation (ID-IS) and multi-stage internal standardisation. Geostand. Geoanalytical Res. 30, 245–271. https://doi.org/10.1111/j.1751-908X.2006.tb01066.x.

Mazzullo, J., Gilbert Grahma, A., Braunstein, C., 1988. Handbook for shipboard sedimentologists, Handbook for shipboard sedimentologists. https://doi.org/http://dx.doi.org/10.2973/odp.tn.8.1988.

Menendez, A., James, R.H., Roberts, S., Peel, K., Connelly, D., 2017. Controls on the distribution of rare earth elements in deep-sea sediments in the North Atlantic Ocean. Ore Geol. Rev. 87, 100–113. https://doi.org/10.1016/j.oregeorev.2016.09.036.

Nakamura, K., Machida, S., Okino, K., Masaki, Y., Iijima, K., Suzuki, K., Kato, Y., 2016. Acoustic characterization of pelagic sediments using sub-bottom profiler data: Implications for the distribution of REY-rich mud in the Minamitorishima EEZ, western Pacific. Geochem. J. 50, 605–619. https://doi.org/10.2343/geochemj.2.0433.

Nozaki, Y., Alibo, D.S., 2003. Importance of vertical geochemical processes in controlling the oceanic profiles of dissolved rare earth elements in the northeastern Indian Ocean. Earth Planet. Sci. Lett. 205, 155–172. https://doi.org/10.1016/S0012-821X(02)01027-0.

Ohta, J., Yasukawa, K., Machida, S., Fujinaga, K., Nakamura, K., Takaya, Y., Iijima, K., Suzuki, K., Kato, Y., 2016. Geological factors responsible for REY-rich mud in the western North Pacific Ocean: Implications from mineralogy and grain size distributions. Geochem. J. 50, 591–603. https://doi.org/10.2343/geochemj.2.0435.

Pattan, J.N., Rao, C.M., Migdisov, A.A., Colley, S., Higgs, N.C., Demidenko, L., 2001.

Ferromanganese nodules and their associated sediments from the Central Indian Ocean Basin: Rare earth element geochemistry. Mar. Georesources Geotechnol. 19, 155–165.

Paytan, A., Kastner, M., Campbell, D., Thiemens, M.H., 1998. Sulfur isotopic composition of Cenozoic seawater sulfate. Science (80-.) 282, 1459–1462. https://doi.org/10.1126/science.282.5393.1459.

Plank, T., Langmuir, C.H., 1998. The chemical composition of subducting sediment and its consequences for the crust and mantle. Chem. Geol. 145, 325–394. https://doi.org/10.1016/S0009-2541(97)00150-2.

Ratcliffe, K., Wright, M., Montgomery, P., Palfrey, A., Vonk, A., Vermeulen, J., Barrett, M., 2010. Application of chemostratigraphy to the Mungaroo Formation, the Gorgon field, offshore northwest Australia. APPEA J. 50, 371. https://doi.org/10.1071/AJ09022.

Rudnick, R.L., Gao, S., 2014. Composition of the Continental Crust, in: Treatise on Geochemistry. Elsevier, pp. 1–51. https://doi.org/10.1016/B978-0-08-095975-7.00301-6.

Takaya, Y., Hiraide, T., Fujinaga, K., Nakamura, K., Kato, Y., 2014. A Study on the Recovery Method of Rare-Earth Elements from REY-Rich Mud toward the Development and the Utilization of REY-Rich Mud. J. MMIJ 130, 104–114. https://doi.org/10.2473/journalofmmij.130.104.

Takaya, Y., Yasukawa, K., Kawasaki, T., Fujinaga, K., Ohta, J., Usui, Y., Nakamura, K., Kimura, J.I., Chang, Q., Hamada, M., Dodbiba, G., Nozaki, T., Iijima, K., Morisawa, T., Kuwahara, T., Ishida, Y., Ichimura, T., Kitazume, M., Fujita, T., Kato, Y., 2018. The tremendous potential of deep-sea mud as a source of rare-earth elements. Sci. Rep. 8, 1–8. https://doi.org/10.1038/s41598-018-23948-5.

Taylor, S.R., McLennan, S.M., 1985. The continental crust, its composition and evolution: an examination of the geochemical record preserved in sedimentary rocks. Blackwell Scientific.

Terashima, S., Taniguchi, M., Mikoshiba, M., Imai, N., 1998. Preparation of two new GSJ geochemical reference materials: Basalt JB-1b and coal fly ash JCFA-1. Geostand. Newsl. 22, 113–117. https://doi.org/10.1111/j.1751-908X.1998.tb00550.x.

Toyoda, K., Nakamura, Y., Masuda, A., 1990. Rare earth elements of Pacific pelagic sediments. Geochim. Cosmochim. Acta 54, 1093–1103. https://doi.org/10.1016/0016-7037(90)90441-M.

Yasukawa, K., Liu, H., Fujinaga, K., Machida, S., Haraguchi, S., Ishii, T., Nakamura, K., Kato, Y., 2014. Geochemistry and mineralogy of REY-rich mud in the eastern Indian Ocean. J. Asian Earth Sci. 93, 25–36. https://doi.org/10.1016/j.jseaes.2014.07.005.

Yasukawa, K., Ohta, J., Miyazaki, T., Vaglarov, B.S., Chang, Q., Ueki, K., Toyama, C., Kimura, J.-I., Tanaka, E., Nakamura, K., Fujinaga, K., Iijima, K., Iwamori, H., Kato, Y., 2019. Statistic and Isotopic Characterization of Deep-Sea Sediments in the Western North Pacific Ocean: Implications for Genesis of the Sediment Extremely Enriched in Rare-Earth Elements. Geochemistry, Geophysics, Geosystems. https://doi.org/10.1029/2019GC008214.

Yasukawa, K., Nakamura, K., Fujinaga, K., Iwamori, H., Kato, Y., 2016. Tracking the spatiotemporal variations of statistically independent components involving enrichment of rare-earth elements in deep-sea sediments. Sci. Rep. 6, 29603. https://doi.org/10.1038/srep29603.

Yasukawa, K., Ohta, J., Mimura, K., Tanaka, E., Takaya, Y., Usui, Y., Fujinaga, K., Machida, S., Nozaki, T., Iijima, K., Nakamura, K., Kato, Y., 2018. A new and prospective resource for scandium: Evidence from the geochemistry of deep-sea sediment in the western North Pacific Ocean. Ore Geol. Rev. 102, 260–267. https://doi.org/10.1016/j.oregeorev.2018.09.001.

Zhang, J., Nozaki, Y., 1996. Rare earth elements and yttrium in seawater: ICP-MS determinations in the East Caroline, Coral Sea, and South Fiji basins of the western South Pacific Ocean. Geochim. Cosmochim. Acta 60, 4631–4644. https://doi.org/10.1016/S0016-7037(96)00276-1.

Zhou, L., Kyte, F.T., 1992. Sedimentation history of the South Pacific pelagic clay province over the last 85 million years Inferred from the geochemistry of Deep Sea Drilling Project Hole 596. Paleoceanography 7, 441–465. https://doi.org/10.1029/92PA01063.